Mathematical modelling of shallow flows: Closure models drawn from grain-scale mechanics of sediment transport and flow hydrodynamics[1]

Rui M. L. Ferreira, Mário J. Franca, João G. A. B. Leal, and António H. Cardoso

Abstract: Mathematical modelling of river processes is, nowadays, a key element in river engineering and planning. River modelling tools should rest on conceptual models drawn from mechanics of sediment transport, river mechanics, and river hydrodynamics. The objectives of the present work are (*i*) to describe conceptual models of sediment transport, deduced from grain-scale mechanics of sediment transport and turbulent flow hydrodynamics, and (*ii*) to present solutions to specific river morphology problems. The conceptual models described are applicable to the morphologic evolution of rivers subjected to the transport of poorly sorted sediment mixtures at low shear stresses and to geomorphic flows featuring intense sediment transport at high shear stresses. In common, these applications share the fact that sediment transport and flow resistance depend, essentially, on grain-scale phenomena. The idealized flow structures are presented and discussed. Numerical solutions for equilibrium and nonequilibrium sediment transport are presented and compared with laboratory and field data.

Key words: sediment load, sediment concentration, turbulence modelling, debris flow, river morphology, conceptual modelling, mathematical model.

Résumé : La modélisation mathématique des processus fluviaux est aujourd'hui un élément clé de l'ingénierie et de la planification des ouvrages en rivière. Les outils de modélisation des rivières devraient se baser sur des modèles théoriques tirés de la mécanique de transport des sédiments, de la mécanique des rivières et de l'hydrodynamique des rivières. Les objectifs de la présente recherche étaient : (*i*) décrire les modèles théoriques de transport des sédiments, déduits de la mécanique de transport des sédiments à l'échelle granulométrique et de l'hydrodynamique des écoulements turbulents et (*ii*) présenter des solutions à des problèmes spécifiques de morphologie des rivières. Les modèles théoriques décrits peuvent être applicables à l'évolution morphologique de rivières soumises au transport de mélanges de sédiments à granulométrie étendue sous de faibles contraintes de cisaillement et lors d'écoulements géomorphologiques comportant un transport intense de sédiments sous de fortes contraintes de cisaillement. Ces applications ont en commun de se baser sur le fait que le transport de sédiments et la résistance à l'écoulement dépendent en grande partie de la taille des grains. Les structures d'écoulement idéalisées sont présentées et examinées. Des solutions numériques pour le transport de sédiments à l'équilibre et hors d'équilibre sont également présentées puis elle sont comparées aux données de laboratoire et de terrain.

Mots-clés : transporte solide, concentration de sédiments, modélisation de la turbulence, écoulement de débris, morphologie des rivières, modélisation théorique, modèle mathématique.

[Traduit par la Rédaction]

1. Introduction

Still a young discipline, fluvial hydraulics has encompassed two different attitudes in what concerns the treatment of its empirical basis, that is, empirical science and engineering practice. It can be argued that fluvial hydraulics only came into being as a true empirical science with the research program for the study of the physics of sediment transport of H.A. Einstein between 1937 and 1950. The approach characteristic of engineering practice inherits the premodern heuristic attitude of observation / reproduction of apparently successful systems, as in the case of the regime method for the design of stable channels.

Until recently, fluvial hydraulics bore visible unresolved tensions between its applied science and engineering conceptions. In 1956, Thomas Blench complained that the find-

Received 10 June 2008. Revision accepted 16 February 2009. Published on the NRC Research Press Web site at cjce.nrc.ca on 3 November 2009.

R.M.L. Ferreira[2] and A.H. Cardoso. Instituto Superior Técnico, TULisbon, Lisbon 1049-001, Portugal.
M.J. Franca. Department of Civil Engineering and IMAR-Institute of Marine Research, Faculdade de Ciências e Tecnologia-Universidade de Coimbra, Coimbra, Portugal.
J.G.A.B. Leal. Universidade Nova de Lisboa, Lisbon, Portugal.

Written discussion of this article is welcomed and will be received by the Editor until 28 February 2010.

[1]This paper is one of a selection of papers in this Special Issue in honour of Professor M. Selim Yalin (1925–2007).
[2]Corresponding author (e-mail: ruif@civil.ist.utl.pt).

ings of Einstein's program were obtained "from laboratory flumes with trifling flows" and suggested that such findings were of use only in such laboratory flows (Ettema and Mutel 2004). Earlier, in 1937, Meyer-Peter, who had enrolled H.A. Einstein in the modification of the Alpine Rhine reach, described Einstein's doctoral thesis as producing "some intriguing ideas, but not exactly useful for my Alpine Rhine study" (Ettema and Mutel 2004).

Engineering practice and scientific methodology have since travelled the path of reconciliation. Further developments in fluid mechanics, namely, in what concerns turbulent flows and flows of granular material, have provided fluvial hydraulics with the formal apparatus to expand Einstein's research program and to create others (Bagnold 1966; Yalin 1977, 1992; Savage and Hutter 1989).

A most significant contribution for the integration of basic phenomenological knowledge into practical engineering works was the advent of computer-aided mathematical modelling of fluvial processes. Indeed, river modelling tools, constituting a key element in river engineering and planning, rest on conceptual models that incorporate empirical knowledge gathered from the mechanics of sediment transport, river mechanics, and river hydrodynamics. Hence, the quality of the engineering tool ultimately depends on basic research efforts not necessarily designed to answer specific engineering needs.

Bearing this principle in mind, the objectives of the present work are (*i*) to describe closed conceptual models for the simulation of open-channel flows with mobile boundaries and (*ii*) to present mathematical solutions to specific problems. Attention is restricted to open-channel flows susceptible to be described by shallow-flow conservation equations and closure equations developed from grain-scale mechanics of sediment transport and flow hydrodynamics. The closure equations are obtained ultimately by space-averaging variables empirically observed under steady and quasi-uniform flow conditions. Grain-scale phenomena are those whose characterization depends on a space-averaging process for which the length scale is of the order of magnitude of the particles that compose the granular bed and the transported material.

The scope of the work includes the morphologic evolution of rivers subjected to the transport of poorly sorted sediment mixtures at low shear stresses and the characterization of geomorphic flows featuring immature debris flow, i.e., intense sediment transport at high shear stresses. Fluvial flows in which bed-forms can develop fall outside the scope of this work: the space-averaging area required for the characterization of the flow variables would scale with the square of the flow depth (Yalin 1977, p. 226). In particular, flow resistance in rivers with dunes owes much to dune-scale form drag (Nelson et al. 1993) and, hence, is not a grain-scale phenomenon.

Much research has been carried out in the characterization of sediment mechanics and hydrodynamics and in ameliorating simulation tools. The work of Yalin (1963, 1977) and Neill and Yalin (1969) on the mechanics of sediment transport deserves a special mention here. Making extensive use of dimensional analysis, Yalin (1977) granted Fluvial Hydraulics a sound theoretical body for the study of initiation of motion, bedload transport, and flow resistance in mobile bed channels. His critique of earlier works on the mechanics of sediment transport, notably those of Meyer-Peter and Müller (1948), Einstein (1950), and Bagnold (1966), remains a fundamental reference in the study of sediment transport phenomena.

The research efforts presented in this text make use of Yalin's (1971, 1977) approach for the description of two-phase phenomena, namely the use of dimensional analysis to isolate the most relevant variables. Under these general guidelines, the structure of flows in coarse-bedded streams and of flows that feature dense mixtures of fluid and sediment are presented and discussed. Flow hydrodynamics and the mechanics of transport of poorly sorted mixtures of sand and gravel are merged into a conceptual model for the morphological and textural evolution of coarse-bedded rivers. Theories dealing with dense granular flows are synthesized, ultimately concurring to a coherent theoretical body capable of describing immature debris flows and, in general, highly sheared water and sediment mixtures. Numerical solutions for the transport of gravel and sand mixtures are presented and compared with laboratory results. Dam-break field data are employed to test the conceptual model for geomorphic flows.

2. Multiple-layer description of the physical systems

2.1. Flow structure of coarse-bedded streams with weak sediment transport

Coarse-bedded streams undergoing weak sediment transport as contact load exhibit a layered flow structure (Nikora et al. 2001; Pokrajac et al. 2008; Ferreira et al. 2009). Should the relative submergence be sufficiently high to allow for the existence and overlap of inner and outer regions, the structure of the flow is essentially that of hydraulically rough fixed beds (Townsend 1976). Nevertheless, in mobile beds, there are aspects that need further clarification, namely the location of the origin of the vertical coordinate and the sub-partition of the inner region, as a function of the nature of the flow variables and taking into consideration the dynamic effects of sediment transport.

The flow structure explained herein is valid for flows with moderate to high relative submergence with overlapping of inner and outer regions. There should not be a universal threshold of the value of the relative submergence that guarantees the existence of inner and outer flow regions. As an example, Ferreira (2008), performing laboratorial work with gravel beds with $d_{50} = 0.06$ m, found that such flow structure could be observed for relative submergences as low as $h/d_{90} \approx 2.5$.

The vertical structure of the flow can be idealized by recognizing the nature of the dominant stresses and momentum sinks. The fluid stress tensor is $\boldsymbol{T}_{ij}^{(w)} = -\rho^{(w)}\phi\langle\overline{u'w'}\rangle - \rho^{(w)}\langle\tilde{u}\tilde{w}\rangle$, where $i,j = x, y, z$ (longitudinal, lateral, and vertical coordinates, respectively), $-\rho^{(w)}\phi\langle\overline{u'w'}\rangle$ are the Reynolds stresses, $-\rho^{(w)}\phi\langle\tilde{u}\tilde{w}\rangle$ are the form-induced stresses, u and w are the longitudinal and vertical velocities, ϕ is the fraction of voids in the bed (Ferreira et al. 2009), the overbar stands for time-average, the prime for fluctuation around the average, the bracket operator for spatial average, and the tilde for spatial variation (Giménez-Curto and Corniero Lera 1996; Finnigan 2000; Nikora et al. 2001). Viscous stresses are considered negligible, as gravel

Fig. 1. Idealized structure of the physical system for coarse-bedded streams. The relevant flow layers are described in the paper. The profiles of the longitudinal mean velocity and the shear stresses and drag forces per unit bed area are based on actual laboratory data by Ferreira et al. (2008).

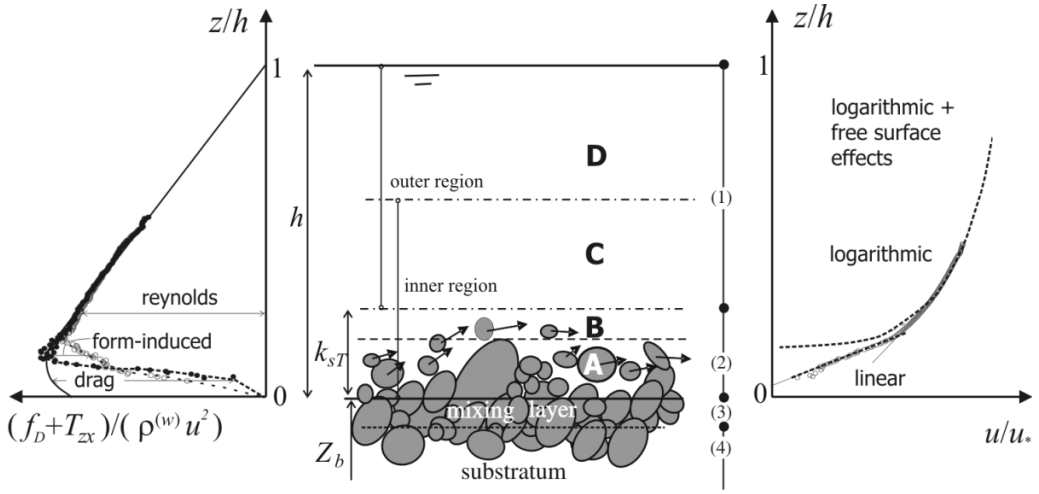

Fig. 2. Computed profiles of relevant nondimensional ensemble-averaged quantities in the transport layer. (*a*) Velocity of the granular constituent, calculated (——) and power-law adjustment (- - - - -); (*b*) solid fraction; (*c*) granular temperature; (*d*) parameter $\Re$; (*e*) parameter Σ and (*f*) parameter Υ. Simulations 1, 2, and 3 correspond to $Y = 1.74$, $Y \approx 2.49$, and $Y \approx 3.07$, respectively, where $Y = u_*^2/\left(g(s-1)d\right)$ is Shields parameter.

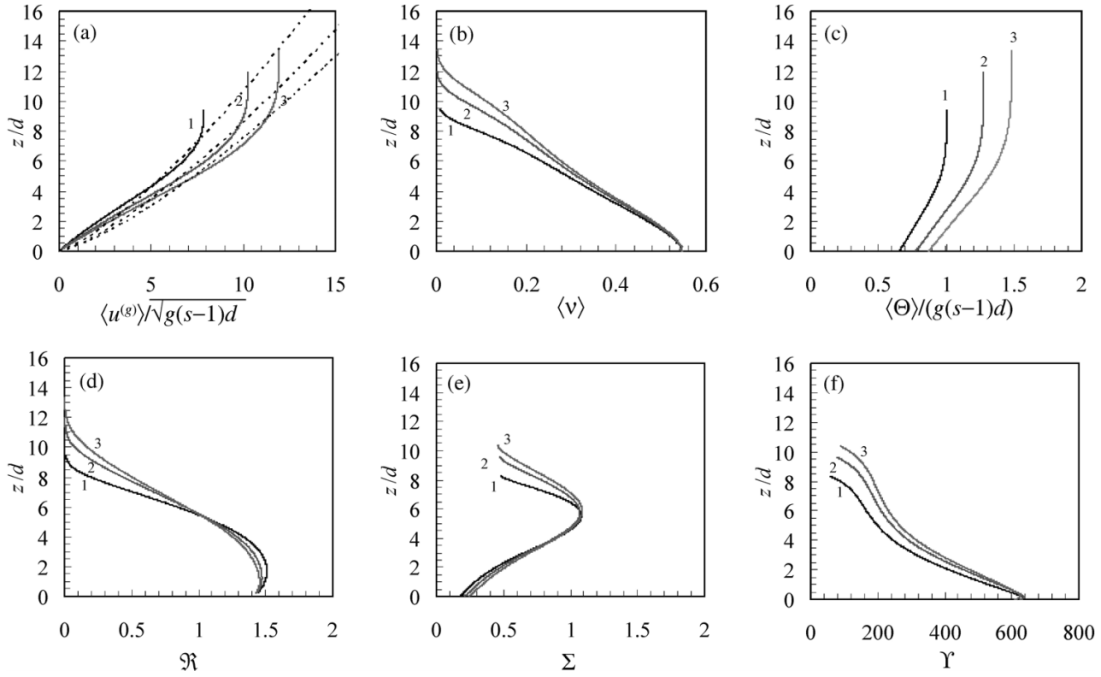

beds are hydraulically rough. Form (or pressure) drag and viscous drag on the bed elements ($f_D^{(w)}$) and drag on moving bedload particles ($f_D^{(gw)}$) are sinks on the equation of conservation of momentum (all drag forces considered are per unit bed area).

Four flow layers are proposed: **A** — pythmenic layer; **B** — interfacial layer; **C** — logarithmic layer; and **D** — free-surface layer (Fig. 1). The pythmenic layer is enclosed by the plane of the highest crests of the bed elements and the plane of the lowest troughs. Pressure and viscous drag ($f_D^{(w)} + f_D^{(gw)} = f_D$ in Fig. 1) become predominant towards the bottom of this layer. Form induced stresses are not negligible for sediment transport rates. Form-induced stresses (Giménez-Curto and Corniero Lera 1996; Finnigan 2000; Nikora et al. 2001; Nikora 2008) are bound to decrease as sediment transport increases (Ferreira 2008; Ferreira et al. 2009) because the spatial correlation necessary for its existence is reduced by bed mobility. In this case, drag over moving particles should be predominantly feeding on form-induced and Reynolds stresses (Ferreira et al. 2009).

The origin of the vertical coordinate z coincides with the bottom boundary of the pythmenic layer, i.e., it is the plane of the lowest troughs in the bed surface (Fig. 1). In this referential, the velocity profile in this region appears to be linear (Nikora et al. 2001) even if there is sediment transport (Ferreira et al. 2009).

Fig. 3. Idealized structure of the physical system as a layered granular / fluid medium. The relevant flow regions are identified in this paper.

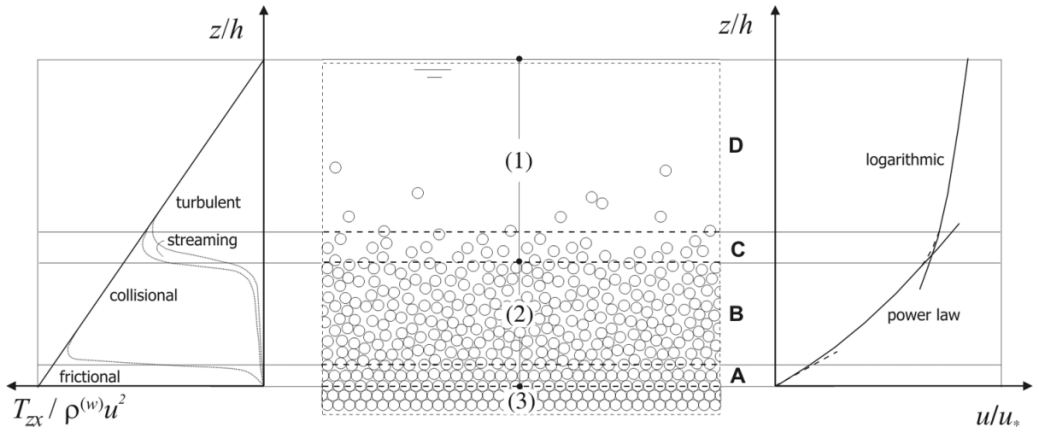

Situated above the particles crests, the interfacial layer is dominated by Reynolds stresses. However, form-induced stresses are seen to subsist (Aberle 2006; Aberle et al. 2008; Pokrajac et al. 2008; Ferreira et al. 2009) and, in the presence of sediment transport, drag on moving particles represents a sink in the equation of conservation of momentum of the fluid constituent.

For computational purposes, the ensemble of layers **A** and **B** constitutes layer (2) whose thickness is k_{sT} (Fig. 1), termed roughness layer, in the absence of sediment transport (Nikora et al. 2001), or bedload layer, in its presence. It will be assumed that the saltation height is approximately equal to the thickness of the region directly influenced by the bed elements and sediment transport.

The overlapping of the inner and outer flow regions is termed layer **C** in Fig. 1. Reynolds stresses are dominant and the nondimensional shear rate $(z/u_*)\mathrm{d}\langle\bar{u}\rangle/\mathrm{d}z$, where $u_* = \sqrt{\tau_b/\rho^{(w)}}$ and τ_b is the bed shear stress, exhibits complete similarity with respect to inner and outer scales if sediment transport is low or inexistent, allowing for the derivation of the logarithmic law for the vertical profile of the longitudinal velocity (Barenblatt 1996; Ferreira 2005; Koll 2006). Self-similarity breaks down at higher transport rates but the profiles, influenced by the magnitude of sediment transport and by the bed surface mixture, should remain logarithmic (Ferreira et al. 2008, 2009).

If the relative submersion is not high, it is still possible to observe the existence of a region, above the crests of the protruding particles, where a logarithmic law still holds, provided that the parameters of the low-log are modified (Dittrich and Koll 1997; Franca and Lemmin 2004; Koll 2006; Franca et al. 2008) or if kinematic scales other that u_* are used.

Layer **D** corresponds to the upper layer of the outer region, where free-surface effects should be included in the equation for the longitudinal velocity profile and where the stress tensor is composed of Reynolds stresses only. Layers **C** and **D** are merged in computational layer (1).

For computational purposes, the bed elevation, Z_b, is defined as the elevation of the plane of the lowest troughs in a referential whose vertical coordinate has a arbitrary origin. If the bed is composed of a poorly sorted sediment mixture, further computational layers must be introduced below the elevation of the lowest troughs. Computational layer (3) is the mixing layer, after Hirano (1971), where sediment exchange between the substratum, layer (4), and the bedload layer (2) occurs. The introduction of layer (3) allows for explicit consideration of vertical sediment fluxes. Acting like a filter, this layer controls both the incoming fractions to the bed and the outgoing fractions to the transport layer (Hirano 1971; Cui et al. 1996). The substratum is a passive layer where sediments are stored. For computational purposes, this may be discretized in layers parallel to the plane of the bed.

2.2. Flow structure of immature debris flows

These flows feature a more complex interaction between moving particles, bed, and fluid. Simple relations for the stress tensor are not possible without a good number of approximations and hypothesis (Savage and Hutter 1989; Jenkins and Richman 1985; Jenkins and Hanes 1998; Pöschel et al. 2002). Generalizing Yalin's (1971, 1977) analysis of the fundamental variables for the study of two-phase phenomena, it is argued, after Iverson (1997) and Ferreira (2005), that stresses in a dense, poorly sorted mixture of fluid and cohesionless sediment particles obey the functional dimensional relation

$$[1] \qquad T = f\left(\zeta, e, \varphi, \langle\nu\rangle, d, \langle\mathrm{d}u/\mathrm{d}z\rangle, \langle\Theta\rangle, \rho^{(w)}, \rho^{(g)}, R, \mu^{(w)}\right)$$

where $\zeta = h_b - z$ is the normal (perpendicular to the plane of the bed) coordinate measured from the top of the transport layer, h_b is the thickness of the transport layer, z is the normal coordinate (measured from the bed), e is the normal coefficient of restitution, φ is the dynamic internal friction angle, $\langle\nu\rangle$ is the solid fraction, d is the representative grain diameter, $\langle\mathrm{d}u/\mathrm{d}z\rangle$ is the shear rate, $\langle\Theta\rangle$ is the granular temperature (defined as the sum of the square of the grain velocity fluctuations, measures the state of agitation of the granular medium, Ogawa (1978), $\rho^{(w)}$ and $\rho^{(g)}$ are the fluid and particle densities, respectively, $R = g(\rho^{(g)} - \rho^{(w)})$ is the submerged weight of particles per unit volume and $\mu^{(w)}$ is the fluid viscosity. If the solid fraction near the bed is high ($> \approx 20\%$), a first hypothesis, included in relation shown in eq. [1], is that turbulent stresses are negligible vis-a-vis other type of stresses, namely those originated in the granular phase (Iverson 1997).

Choosing d, $\langle\mathrm{d}u/\mathrm{d}z\rangle$, and R as basic variables, applying the Vaschy-Buckingham theorem, and combining the resulting nondimensional parameters, one obtains

$$[2] \qquad \frac{T}{\rho^{(w)} d^2 \langle\mathrm{d}u/\mathrm{d}z\rangle^2} = \prod\left(\frac{\zeta}{d}, e, \varphi, \langle\nu\rangle, \Re, s, \Sigma, \Upsilon\right)$$

where $s = \rho^{(g)}/\rho^{(w)}$ is the specific gravity of the transported

sediment. Parameters $\Re$, Σ, and Υ can be employed to characterize the structure of the transport layer. They account for the influence of (*i*) binary collisions as a means to transfer momentum between moving particles and source of collisional stresses (Jenkins and Savage 1983; Lun et al. 1984; Jenkins and Richman 1985, 1988), (*ii*) streaming motion, i.e., particle velocity fluctuations in the interval between collisions or other interaction with other particles, source of streaming stresses (Jenkins and Richman 1988; Campbell 1989), (*iii*) enduring frictional contacts among particles and particles and the bed, source of frictional stresses (Savage 1979; Savage and Hutter 1989), and (*iv*) fluid viscosity (Armanini et al. 2005; Ferreira 2005).

Parameter $\Re = d\langle \mathrm{d}u/\mathrm{d}z\rangle\langle\Theta\rangle^{-1/2}$ (Savage and Jeffrey 1981; Lun et al. 1984), the "shear efficiency number" (Ferreira 2005), is a measure of the correlation between the generation of collisional stresses and the state of agitation of a granular flowing system. It can also be interpreted as a measure of the efficiency of the shear work in generating a particular state of agitation, measured by the granular temperature. Parameter $\Sigma = \rho^{(w)} d^2 \langle \mathrm{d}u/\mathrm{d}z\rangle^2/(R\langle\nu\rangle\zeta)$, the Savage number (Savage and Hutter 1989), acquired relevance after Savage (1979), in the context of the study of the flow of granular material obeying a Coulomb–Mohr rheology. It represents the ratio of collisional stresses to frictional stresses. The former is identified by the quadratic dependence on the shear rate and the later is indirectly represented by the submerged weight, per unit bed area, of granular material. Parameter $\Upsilon = R\langle\nu\rangle\zeta\tan(\varphi)/\left(\mu^{(w)}\langle \mathrm{d}u/\mathrm{d}z\rangle\right)$ (Iverson 1997) expresses the relation between stresses born by long-term frictional interactions and fluid viscous stresses.

Ferreira (2005), following Jenkins and Hanes (1998), performed a theoretical study of the transport layer of a sloping bed with intense transport. Considering a two-dimensional (2-D) vertical flow of a dense mixture of fluid and sediment, the equations of conservation of momentum of the fluid and of the granular phase and the equation of conservation of the particle fluctuating energy were solved numerically subjected to appropriate boundary conditions. A detailed account of the solution procedure and of the boundary conditions can be found in Ferreira (2008). The most important aspects can be summarized as follows. At $z = 0$, (*i*) the granular pressure is the submerged weight, per unit area, of the volume of granular material and the granular shear stresses are frictional and equal to the granular pressure multiplied by $\tan(\varphi_b)$, where φ_b is the friction angle at the bed; (*ii*) the no-slip condition applies to fluid and granular velocities; (*iii*) the solid fraction is equal to the reciprocal of the porosity; (*iv*) the granular temperature is calculated from a granular equation of state (Lun et al. 1984; Jenkins and Richman 1985, 1988), given the granular pressure; and (*v*) the flux of fluctuating energy follows from a modification of the solution of Jenkins and Askari (1991) across the bottom boundary to account for frictional effects (Ferreira 2005). At $z = h_b$, (*i*) the flux of fluctuating energy, the solid fraction, and the granular pressure are zero. The shooting method employed to solve the system requires that h_b and $e^{(gw)}$, the submerged coefficient of restitution, are unknown parameters (Ascher et al. 1995). The constitutive equations for the granular stress tensor are derived from the dense limit of the kinetic theory of gases (Chapman and Cowling 1970), introducing energy dissipation by inelastic collisions (Jenkins and Richman 1985, 1988) and due to fluid viscosity (Ferreira 2005). Selected results of the numerical simulations as well as the profiles of $\Re$, Σ, and Υ, are displayed in Fig. 2.

Low values of $\Re$ are typical of diluted systems (low-solid fraction), where streaming stresses are dominant; values of the order of the unity signify that collisional stresses prevail over streaming stresses. It is seen in Fig. 2*d* that $\Re$ increases towards the bed, where a given shear rate (Fig. 2*a*) produces a small amount of granular temperature (Fig. 2*c*); on the contrary, in the diluted upper regions of the transport layer (Fig. 2*b*), the same shear rate is likely to produce an intense state of agitation. Low values of Σ are associated to a predominance of frictional stresses over collisional. Observing Fig. 2*e*, it is expected that frictional stresses prevail near the bed. Parameter Σ is O(1), where collisional stresses dominate. Large / (small) values of Υ signal the preponderance of frictional / (viscous) stresses over viscous / (frictional). Figure 2*f* shows that, at the bottom of the transport layer, frictional stresses are more important than viscous. However, in the core of the transport layer, the influence of fluid viscosity is never negligible as seen by the fast decrease of Υ with z.

Figure 3 synthesizes the information relative to the structure of stress-production mechanisms. An idealization of the mean (time-averaged) velocity profile is also shown. Granular frictional stresses are dominant near the bed, in the frictional layer (**A**). Above, the core of the transport layer, is designated by collisional layer (**B**), where collisional stresses are dominant but viscous stresses play a nonnegligible role (Ferreira 2005). At the top of the transport layer, a transition layer exists (**C**), where streaming stresses dominate over collisional. For a small quantity of particles moving in a turbulent flow of a viscous fluid, as is the case in the upper region of layer **C**, it is assumed that the degree of freedom between the fluid motion and the particle motion is small and that streaming stresses are small compared with Reynolds stresses.

For computational purposes, layer (1) includes the uppermost flow layer (**D** in Fig. 3) and the transitional layer **C**. In these layers, the velocity profile is approximately logarithmic and dominated by turbulent stresses. Computational layer (2), identifiable with the transport layer, is composed of layers **A** and **B**. As discussed in Sect.3.2.1, the velocity profile is well adjusted to a power law.

Computational layer (3) corresponds to the bed, where grain movement is reduced to its state of agitation. For computational purposes, the bed elevation, relative to an arbitrary horizontal plane, is defined as the bottom boundary of the frictional layer **A**, i.e., the elevation of the uppermost layer of particles that have no longitudinal movement.

2.3 Multiple-layer modelling: Equations of conservation

Multiple-layer conceptual approaches interpret flow variables as depth-averaged quantities, integrated over layer thicknesses. This approach achieves a balance between computational simplicity of depth-averaged models and phenomenological complexity of three-dimensional (3-D) descriptions by addressing explicitly vertical exchange processes between layers.

To develop a conceptual model within the multiple-layer paradigm, it is necessary that the corresponding physical systems (*i*) have a layered structure, e.g., different stress mechanisms or sediment concentrations at different levels

and (*ii*) are susceptible to be described by an equivalent continuum of granular material and fluid mixture.

Conservation equations for the layered systems described in the previous sections can be derived by depth integrating the two-dimensional vertical (2-DV) conservation equations for each of the phases within the continuum hypothesis (details in Ferreira 2005). In one-dimensional (1-D) cases, the overall mass conservation equation is

$$[3] \qquad \partial_t(h + Z_b) + \partial_x(uh) = 0$$

where u is the depth-averaged flow velocity, Z_b is the bed elevation, and t and x are the time and space coordinates, respectively. The sediment mass conservation equations in layer (2) are

$$[4] \qquad \partial_t\left(\widehat{C}_k^{(2)} h_b\right) + \partial_x(C_{b_k} u_b h_b) - \phi^{net}_{s_k\,3,2} = 0$$

where u_b is the velocity of layer (2), $\phi^{net}_{s_k\,3,2}$ is the net rate of sediment mass of size fraction k exchanged between layers (2) and (3), $\widehat{C}_k^{(2)}$ is the depth-averaged concentration of size fraction k in (2) and C_{b_k} is the flux-averaged concentration of size fraction k in (2).

In layer (3), the mixing layer, conservation of each size fraction in the mixing layer is

$$[5] \qquad (1-p)\ \partial_t(L_a F_k) + \phi^{net}_{s_k 3,2} - \phi^{net}_{s_k 4,3} = 0$$

where p is the bed porosity, L_a is the thickness of the mixing layer, F_k is the percentage of the size fraction k in the mixing layer, and $\phi^{net}_{s_k}$ is the net rate of sediment mass of size fraction k exchanged between the mixing layer and the substratum. The mass conservation equation in the bed is

$$[6] \qquad (1-p)\partial_t(Z_b) + \phi^{net}_{s\ 3,2} = 0$$

where $\phi^{net}_{s\ 3,2}$ is the net rate of sediment mass exchanged between layers (2) and (3). It is implied by eqs. [4], [5], and [6] that $\phi^{net}_{3,2}$ is the net rate of mass exchanged between layers (2) and (3) and that $\phi^{net}_{3,2} = \phi^{net}_{s3,2}/(1-p)$.

The equation of conservation of momentum is obtained by summing the corresponding momentum equations of each of the layers. It is implicit that the velocity and the shear stress profiles are continuous across the boundary between layers (1) and (2) (refer to Ferreira 2005, Sect. 3 for details). The result is

$$[7] \qquad \partial_t(\rho_m uh) + \partial_x\left(\rho_b {u_b}^2 h_b + \rho^{(w)} {u_w}^2 h_w\right) + \frac{1}{2} g \partial_x\left(\rho^{(w)} {h_w}^2 + \rho^{(w)} h_w h_b + 2\rho_b {h_b}^2\right) = -g\left(\rho_b h_b + \rho^{(w)} h_w\right)\partial_x(Z_b) - \tau_{3,2}$$

where $h_w = h - h_b$ is the thickness of layer (1), $u_w = (uh - u_b h_b)/(h - h_b)$ is the velocity of layer (1), $\rho_m = \rho^{(w)}\,[1 + (s-1)C]$ is the mean flow density, $\rho_b = \rho^{(w)}\,[1 + (s-1)C_b]$ is the density of layer (2), $C = C_b u_b h_b/(uh)$ is the mean flux-averaged concentration of sediment, C_b is the flux-averaged sediment concentration in (2) and $\tau_{3,2} \equiv \tau_b$ is the force per unit area between layers (2) and (3) (bed shear stress).

The system of partial differential eqs. [3–7] has $3 + n + (n-1)$ unknowns, where n is the number of size fractions in the bed. These unknowns are the flow elevation $Z_s = h + Z_b$, the mass discharge per unit width $R_m = \rho_m uh$, Z_b, C_{b_k} for $k = 1,\ldots, n$, and F_k for $k = 1,\ldots, n-1$, where, naturally, $\sum_k F_k = 1$.

The next section is dedicated to present the closure equations for h_b, u_b, C_b, L_a, $\phi^{net}_{s_k\,3,2}$, and $\phi^{net}_{s_k}$ that complete the conceptual models.

3. Conceptual models for the transport layer

3.1. Coarse-bedded streams with weak sediment transport

3.1.1. Thickness and velocity of the bedload layer

It is assumed that the thickness of the bedload layer is the distance between the elevation of maximum of the zenith of the saltation paths and the elevation of the troughs of the bed. Modifying Owen's (1964) analysis, it is considered that the maximum potential energy of a saltating particle equals its kinetic energy at entrainment minus the work of the drag force during its vertical excursion plus (or minus, if the particle is faster than the surrounding flow) the work of the lift force:

$$[8] \qquad \rho^{(w)}(s-1)d_m^3 C_V g z_{max} = \frac{1}{2}\rho^{(w)} s d_m^3 C_V w_0^2 - \frac{1}{2}\rho^{(w)} d_m^2 C_1 C_D w_0^2 z_{max} + \frac{1}{2}\rho^{(w)} d_m^2 C_1 C_L \langle\left(u^{(w)} - u^{(g)}\right)|u^{(w)} - u^{(g)}|\rangle z_{max}$$

where z_{max} is the height above the rest point that is attained by the particle performing the higher jumps, d_m is the diameter of the particle that performs the higher jumps, C_V is the ratio of the actual particle volume to the volume of a sphere whose diameter is d_m, C_{11} is the ratio of the larger particle axis to d_m, w_0 is the initial vertical particle velocity, and $\langle\left(u^{(w)} - u^{(g)}\right)|u^{(w)} - u^{(g)}|\rangle$ is the average lag velocity between the particle (superscript g) and the surrounding fluid (superscript w).

It is implicit in eq. [8] that the work of drag in the longitudinal direction affects the jump length, not the jump height. Considering the particle that attains the highest position above the bed is entrained at an elevation of d_{90} from the lowest trough and both the particle and the fluid velocities are expressed as $\langle\left(u^{(w)} - u^{(g)}\right)|u^{(w)} - u^{(g)}|\rangle = m_u(u_*^2 - u_{*ref}^2)$ and $w_0^2 = m_w(u_*^2 - u_{*ref}^2)$, we obtain

$$[9] \qquad \frac{h_b}{d_{90}} = 1 + \frac{\frac{1}{2}s(d_m/d_{90})C_V m_w(Y_{50} - Y_{ref})}{(d_m/d_{90})C_V + \left(\frac{1}{2}C_1 C_D m_w - \frac{1}{2}C_1 C_L m_u\right)(Y_{50} - Y_{ref})}$$

Fig. 4. (*a*) Path- and ensemble-averaged grain velocities. White circles (○) stand for the laboratorial data for each size fraction ($u^{(g)}$); black circles (●) stand for the average over all size fractions (u_{cb}). Line indicates for eq. [10], the best fit over all size fractions. (*b*) Thickness of the bedload layer. Black circles (●) stand for the measured thickness; thick line indicates eq. [9]; thin line stands for $h_b/d_{90} = 73Y_{50}/(1 + 18.5Y_{50})$.

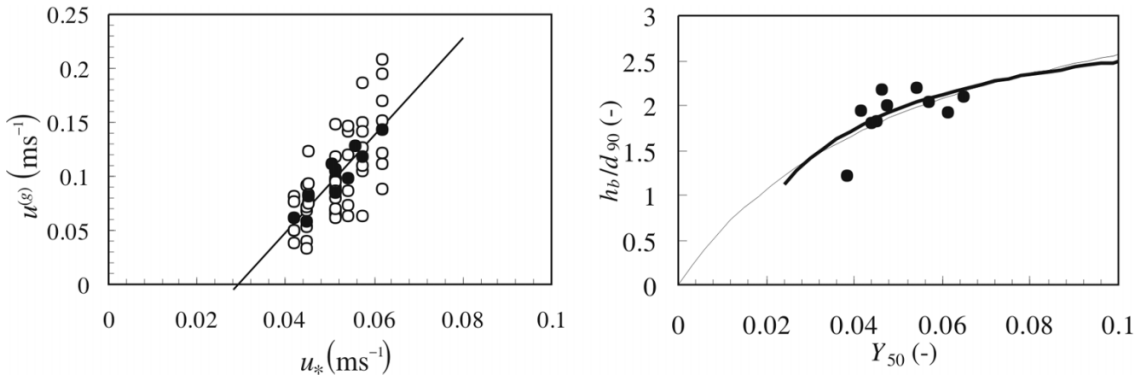

Fig. 5. Time- and ensemble-averaged longitudinal fluid velocity profiles (○) for four uniform, capacity, laboratory tests. (*a*) $Fr = 0.40$, $Y_{50} = 0.021$, $k_s^+ = k_s u_*/\nu = 153$; (*b*) $Fr = 0.43$, $Y_{50} = 0.026$, $k_s^+ = 157$; (*c*) $Fr = 0.60$, $Y_{50} = 0.039$, $k_s^+ = 227$; (*d*) $Fr = 0.61$, $Y_{50} = 0.050$, $k_s^+ = 346$. Full line indicates eq. [11]. Dotted line indicates the logarithmic law.

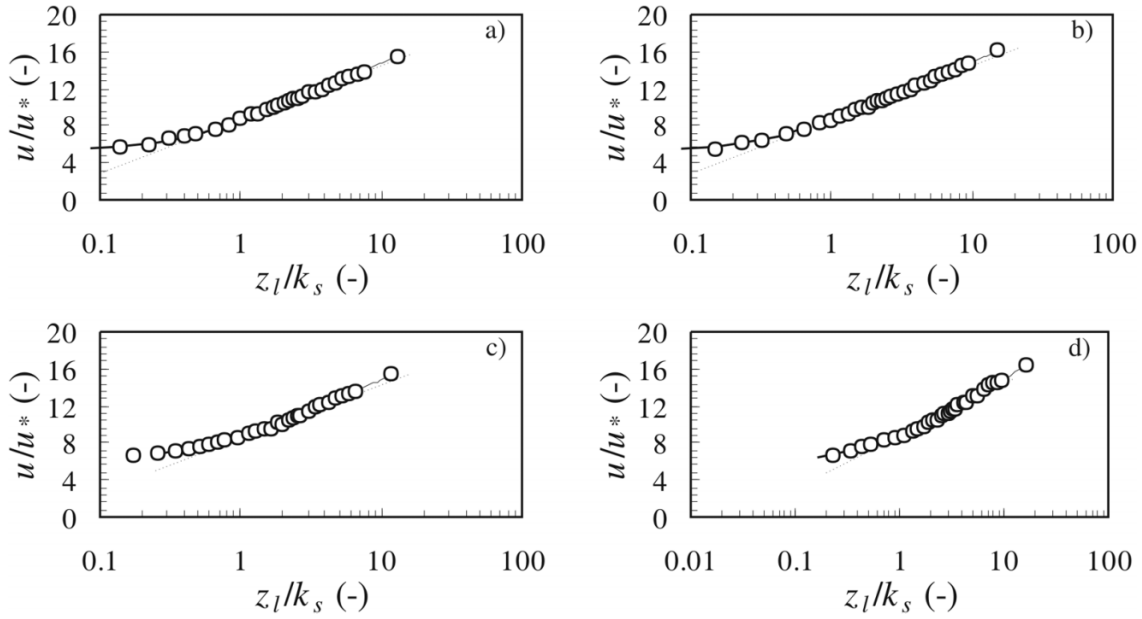

Fig. 6. Partition of the flow energy through the different scales of a wavelet multi-level decomposition; results obtained at one point within the boundary layer of a gravel-bedded stream (after Franca 2005, Sect. 3.6).

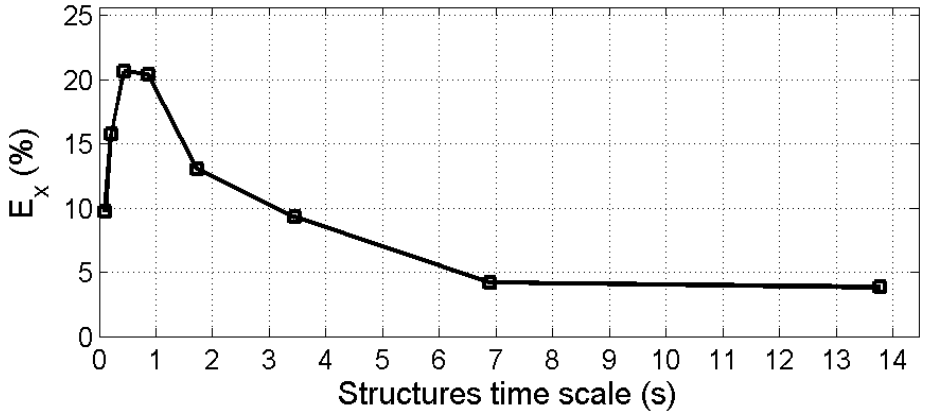

Fig. 7. (*a*) Three-dimentional (3-D) reconstruction of a bursting cycle, sampled through wavelet-based multilevel decomposition (time normalized by event duration and velocities normalized by difference of the maximum and minimum event velocities detected for the most energetic scale, details in Franca 2005, Section 3.6); points 1 and 5 are the beginning and end of the cycle. (*b*) Distribution of the time period between consecutive events (after Franca and Lemmin 2006).

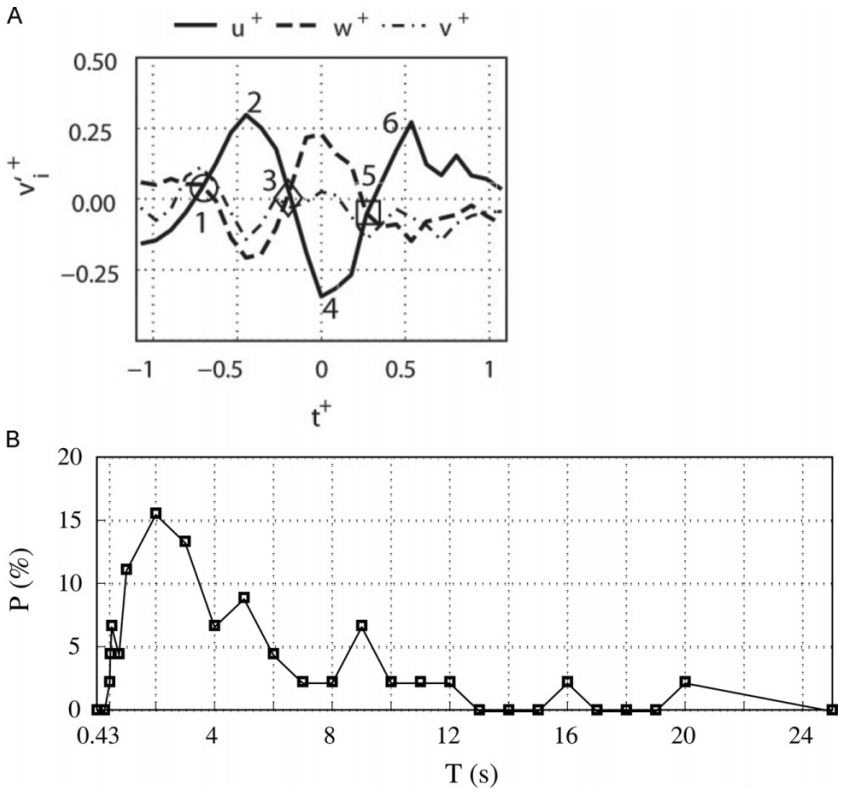

Fig. 8. Nondimensional bedload volumetric discharge rates as a function of the nondimensional shear stress. Equation [14] (- - -) plotted against laboratorial data of Ferreira (2005). Size fractions, in mm: 6.9 (×), 5.55 (●), 4.0 (▲), 3.09 (◆), 2.4 (■), 1.85 (○), 1.5 (△), 1.2 (◊) and 0.93 (□).

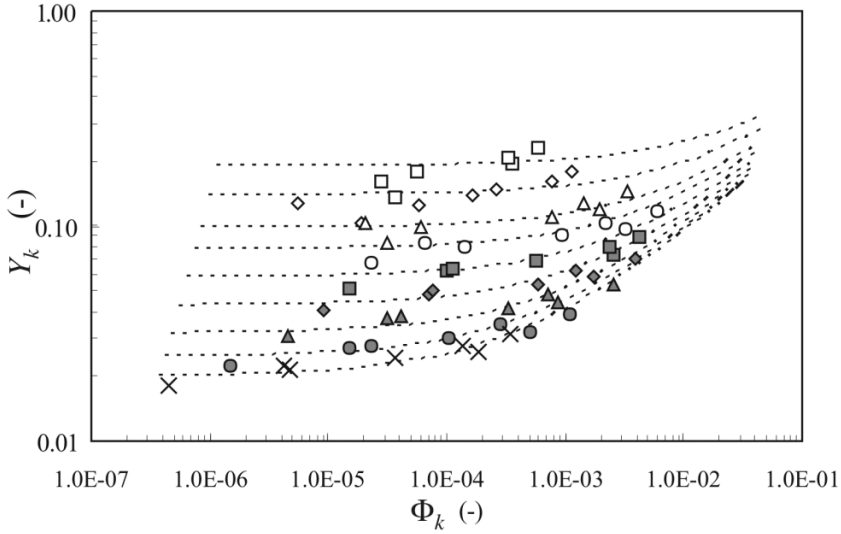

where $Y_{50} = u_*^2/(g(s-1)d_{50})$ is the Shields parameter computed with the median diameter d_{50}, Y_{ref} is a reference value of Shields' parameter such that $Y_{50} < Y_{\text{ref}} \Rightarrow h_b = d_{90}$. From the shape data presented in Ferreira et al. (2007), C_V = 1.0, C_1 = 1.2. Laboratory data, presented in Ferreira (2005), obtained with d_m = 2.3 mm and $d_{90} \approx 5.0$ mm, allows one to compute $u_{*\text{ref}} = 0.029$, Y_{ref} = 0.022, and $m_u \approx 10$ (see also Figs. 4*a* and 5). Considering that C_D = 0.4 and C_L = 0.2 (Ferreira et al. 2007), we found that the angle at which the particle leaves the bed and its modulus by minimizing the mean square error between the computed values and the values drawn from the laboratory data of Ferreira (2005). The experimental results and fitted eq. [9] are displayed in Fig. 4*b*.

Fig. 9. Friction factor defined as $C_f = (u_*/u)^2$. Equation [15] (——) is superimposed to laboratorial data: mobile sand–gravel bedded tests (◊); armoured sand–gravel bedded tests (◆), and mobile and sub-threshold gravel bedded tests (○).

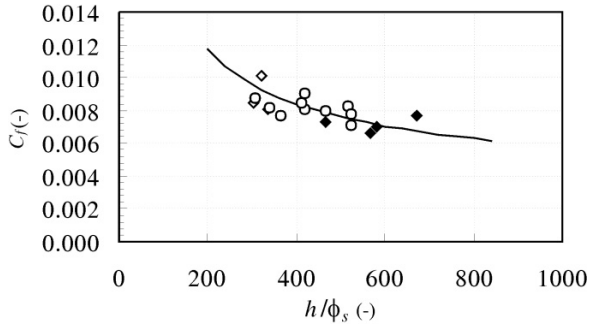

Fig. 10. Thickness of the transport layer as a function of Shields parameter. Sensitivity analysis to the characteristics of the sediment grains. The four types of granular material used by Sumer et al. (1996), were plastic (d = 0.003 m, s = 1.27, e = 0.75 and d = 0.0026 m, s = 1.14, e = 0.75), acrylic (d = 0.0006 m, s = 1.13, e = 0.75) and sand (d = 0.00013 m, s = 2.67, e = 0.8); ν_0 = 0.6; tan(φ_b) = 0.4; q = 1.0 m^2/s. Circles (○) stand for Sumer et al. data.

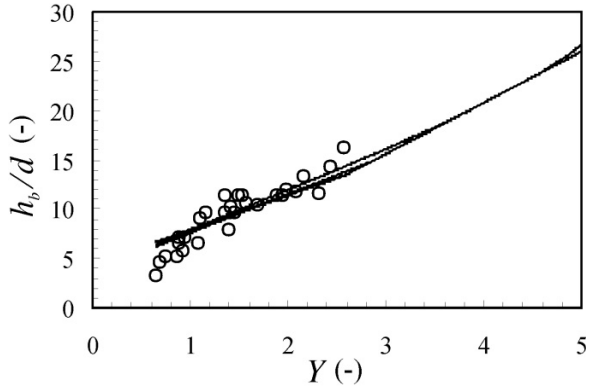

The fitting procedure led to m_w = 47.1 and an initial flight angle of 45°, which means that the horizontal velocity at the moment of entrainment is of the order of magnitude of $10u_*$, which is plausible. For computational purposes, it is desirable that $h_b = 0$ when $Y_{50} = 0$. For that reason, the approximate expression $h_b/d_{90} = 73Y_{50}/(1 + 18.5Y_{50})$, also displayed in Fig. 4*b*, is used for small values of Y_{50}.

The velocity of layer (2) is a composition of the mean velocities of the grains moving as bedload (u_{cb}) and the mean velocity of the fluid (u_{wb}). The path- and ensemble-averaged velocity of the particles travelling as bedload (shown in Fig. 4*a* for gravel and sand-size fractions) reveals that single linear function of u_* applies to all size fractions (Ferreira et al. 2006*a*). The latter is

$$[10] \qquad u_{cb} = 4.5(u_* - u_{*ref})$$

where $u_{*ref} = 0.029$ m^{3}s^{-1} is deduced from the coefficients of the linear regression. Equation [10] is comparable to that proposed by Niño et al. (1994).

As for the fluid velocity, the data of Ferreira (2005), allows one to characterize profiles of the longitudinal velocity. Four typical profiles, representing the upper parts of the bedload layer, the logarithmic layer, and the lower parts of the free-surface layer, are shown in Fig. 5. They are a result of a time and an ensemble averaging process: four independent time-averaged profiles are considered for the ensemble average. Nikora et al. (2001) proposed that the time- and space-averaged velocity profile in the roughness layer should be linear in z_l/k_s where $z_l = z - \Delta$, $k_s = k_{sT} - \Delta$, k_{sT} is the characteristic scale of the roughness elements (Fig. 1), and Δ is the displacement height (see Ferreira et al. 2009 for a discussion of the value of these parameters). However, analysis of the experimental data reveals that

Fig. 11. Friction coefficient for immature debris flows. Equation [23] is superimposed to laboratorial data performed with sand (■); acrylic (◊); plastic with d = 0.003 m (●), and plastic with d = 0.003 m and plastic with d = 0.0026 m (○). Remaining sediment characteristics in the caption of Fig. 10.

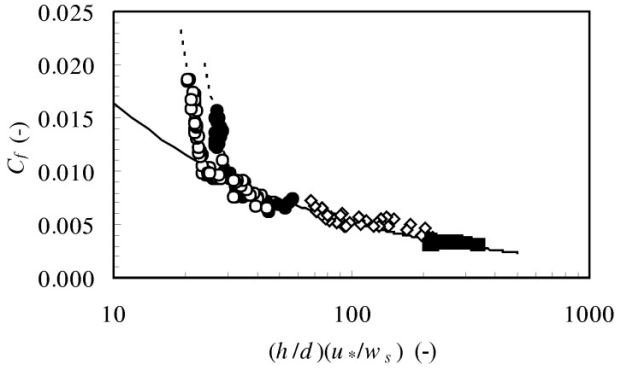

$$[11] \qquad \frac{u(z)}{u_*} = m_1 \frac{z_l}{k_s} + b_1$$

where m_1 = 6.2 and b_1 = 3.4 for the particular mixtures of the laboratorial tests.

It is noted that eq. [11] predicts a slip velocity at $z = \Delta$, i.e., the velocity in the bedload layer cannot be linear throughout its entire thickness. Near the troughs, a zone dominated by flow separation, the time- and space-averaged velocity is probably dependent on the arrangement of the bed surface, rendering m_1 and b_1 dependent on flow variables and on the bed mixture.

The integration of eq. [11] results in $u_{wb} = u_*\{m_1/2 + b_1\}$ if it is assumed that $h_b \approx k_{sT} - \Delta$. The depth-averaged velocity of the fluid in the bedload layer becomes $u_{wb} = 6.5u_*$.

Finally, the velocity in the bedload layer is (refer to Ferreira 2005 for details)

$$[12] \qquad u_b = u_{wb} - \widehat{C}^{(2)}(u_{wb} - u_{cb})$$

where the depth-averaged sediment concentration is $\widehat{C}^{(2)} \approx 2C_b$ for low to moderate concentrations (Ferreira et al. 2006*a*).

3.1.2. Near-bed organised turbulence and detection of sediment driving coherent structures

Intermittent organized motion within the boundary layer, like bursting phenomena, is intrinsically related to transport processes. The characterization of bursting phenomena was put forward by Grass (1971), Nakagawa and Nezu (1977), among others. Recently, experimental results on coherent motion in gravel-bedded flows have been shown by Franca

and Lemmin (2006) from a natural armoured river and by Ferreira et al. (2002) from flow over gravel-sand beds with bedload.

The assessment of the momentum generated by coherent structures needs to account for the duration (time scale) of their cycle. The application of wavelets is suitable to identify and analyze coherent structures in the boundary layer of geophysical flows (Foufoula-Georgiou and Kumar 1994 and others). Wavelet decomposition allows one to evaluate the energy partition throughout the scales present in the instantaneous velocity signal; Fig. 6 is based on results obtained in one point within the boundary layer of a gravel-bedded stream (Franca 2005, section 3.6).

Franca and Lemmin (2006) applied an algorithm of detection and reconstruction of coherent structures based on the wavelet multiresolution analysis to the most energetic scale seen in Fig. 6 (ΔT = 0.43 s), allowing the reconstruction of a bursting cycle (Fig. 7*a*) with a sweep and an ejection scaling both with ΔT. For the positive detection of an event, the comparison of the instantaneous shear stress relative amplitude with threshold value $QH > 5$ was used, where QH is evaluated locally and corresponds to the ratio between the reconstructed shear series within the analysed wavelet scale and its mean value. From the distribution of the time period between the occurrence of the bursting cycle (T), it was found that the observed bursting packets are independent. The intermittency character of the event is represented by T which had an extreme-type statistical distribution (Fig. 7*b*), where the most probable value correspond to T = 2 s. In this case, the persistency factor $\Delta T/T$, a measure of the momentum input from the detected structures, is 0.22.

3.1.3. Equilibrium bedload discharge

The hypothesis that entrainment and transport of sediment particles are related directly to organised turbulence may be traced to the work of Sutherland (1967). Prior to the concept of coherent turbulent events, he performed a landmark study built around the idea that sediment is entrained when a mass of fluid impinges on the bed. In a turbulent flow, the mass of fluid takes the form of a sweep event, which promotes its entrainment by increasing locally the hydrodynamic actions upon the particles past their critical stability values. . This description embodies the concept of event-driven bedload transport. The event-driven sediment transport model developed here is based on those developed by Hogg et al. (1996) and Ferreira (2005), the latter for granulometric mixtures.

It is considered that under small mean shear, the ratio of the bedload concentration during an impinging event to $(Y - Y_c)^{3/2}$ is a constant (where $Y = \rho^{(w)} u_*^2 / \left(g(s-1)d\right)$ is Shields' parameter and Y_c is a critical Shields' parameter). Under this assumption, the bedload discharge is proportional to Y^β, $\beta > 3/2$, a fact experimentally observed by Wilcock et al. (2001) among others. Under this hypothesis one has

$$[13] \qquad \frac{E_k/(F_k A_{IV} H_k)}{(Y_k - Y_{ck})^{3/2}} = c$$

where E_k is the volume of sediment of size fraction k entrained during a sweep event, A_{IV} is the area of influence of the sweep event per unit width, H_k is the thickness of the erodible layer for size fraction k, and c is a constant. The group $F_k A_{IV} H_k$ is the volume of sediment and voids from which the sweep event can extract sediment whereas the group $E_k/(F_k A_{IV} H_k)$ can be interpreted as the sediment concentration that can be locally generated by a sweep event if all particles were of size k. Obviously, by "sweep event" it is meant a statistically representative event, for instance, the expected value of its distribution. Using Taylors' frozen turbulence hypothesis, the area of influence of the event can be written as $A_{IV} = \Delta T\ u_0$, where u_0 is the time- and space-averaged fluid velocity at the level of the crests of the bed elements. An estimation for u_0 comes from eq. [11], $u_0 = 5.2u_*$. The thickness of the erodible layer is a fraction of the thickness of the mixing layer. For the largest grains in the bed, H_k is the full thickness of this layer in the sense that their entrainment implies the removal of a volume of bed material whose height is equal to the thickness of the mixing layer. The entrainment of smaller represents the removal of a thinner equivalent layer of bed material. To account for this hiding effect, a distribution function W_k, approximated by d_k/d_{max}, where d_{max} is the sieving diameter of the larger particle found in the bed surface samples, is introduced. If the thickness of the mixing layer is $L_a = 3d_{50}$, then $H_k = 3d_{50}W_k$. Substituting these definitions and estimates in eq. [13], the volume of sediment of size fraction k entrained by each sweep event is obtained. To know the bedload discharge, it is necessary to know the frequency of the events. Thus, the bedload discharge for each size fraction k, $q^*_{sb_k}$, is obtained by dividing the respective volume by the period, T, of the representative sweep event.

Employing the ratio $\Delta T/T$ = 0.22 previously evaluated in Sect. 3.1.2, eq. [13] becomes

$$[14] \qquad \Phi_k = 3.56 c W_k \frac{d_{50}}{d_k} (Y_k - Y_{ck})^{\frac{3}{2}} Y_k^{\frac{1}{2}}$$

where $\Phi_k = q^*_{sb_k} / \left\{ \left(g d_k (s-1)\right)^{\frac{1}{2}} d_k F_k \right\}$. The values of c = 1.00 and Y_{ck} were determined empirically using Ferreira's (2005) laboratory data for a gravel–sand mixture (details in Ferreira et al. 2007 about Y_{ck}). The graphical expression of eq. [14] can be seen in Fig. 8 along with the laboratory data.

3.1.4. Flow resistance

The friction factor, defined here as $C_f = (u_*/u)^2$, in gravel–sand bedded streams with weak sediment transport can be derived from the logarithmic velocity profile plus eq. [11]. One obtains

$$[15] \qquad C_f = \left\{ 2.5 \ln\left(0.22 \frac{h}{\zeta_s}\right) \right\}^{-2}$$

where the roughness length is $\zeta_s = (k_{sT} - \Delta) e^{-\kappa B}$, B is the constant in the logarithmic law, and κ = 0.41 is the von Kármán constant. The parameters k_{sT} and B were fitted from experimental data with a procedure explained in Ferreira et al. (2008*a*). Equation [15] was superimposed to laboratorial values of C_f, as shown in Fig. 9.

It is underlined that the value of u_* in the definition of C_f includes shear stresses and form drag at the bed. The experimental values of C_f were calculated from $C_f = -g R_h \partial_x(Z_b)/u^2$, where R_h is the bed hydraulic radius, determined with a procedure adapted from Chiew and Parker (1994).

3.1.5. Vertical fluxes and mixing layer

The vertical flux between the substratum and the mixing layer is

$$[16] \qquad \phi^{\text{net}}_{s_k 4,3} = (1-p) f_{I_k} \partial_t (Z_b)$$

The composition of the sediment transferred between these layers is controlled by the transfer function f_{I_k}, the proportion of the size fraction k at the interface (Toro-Escobar et al. 1996). In an aggradational process, the formula of Cui et al. (1996) is used: $f_{I_k} = \beta_I p_k + (1-\beta_I) F_k$, where p_k stands for the composition of the bedload and β_I should be calibrated from existing data (Cui et al. 1996 used 0.7, Ferreira 2005, used 0.3). If erosion is dominant, Hirano's (Hirano 1971) concept holds and $f_{I_k} = f_k$, where f_k is the composition of the substrate. Note that $\beta_I = 0.0$ should not be used because it is incompatible with downstream fining (Parker 1991).

The hypothesis that the flux between the mixing layer and the bedload layer is proportional to the imbalance between capacity and actual bedload discharge is pursued in this work (time and space lag effects). Thus, it can be written

$$[17] \qquad \phi^{\text{net}}_{3,2} = -\frac{q^*_{sb} - C_{b_k} u_b h_b}{\Lambda}$$

where Λ is a geometric scale associated to the length necessary for the attenuation of a given imbalance. Expressions for bedload are given by Phillips and Sutherland (1989) among others but, in general, Λ must be calibrated with experimental data.

3.2. Immature debris flows

3.2.1. Thickness and velocity of the transport layer

An analysis of the numerical results shown in section 2.2, especially Fig. 2, allows one to determine an equation for the velocity of the mixture in layer (2). A good fit to the results in Fig. 2*a* is

$$[18] \qquad \frac{u(z)}{u_*} = 2.1 \left(\frac{\Gamma}{Y}\right)^{3/4} \left(\frac{z}{h}\right)^{3/4}$$

adapted from Sumer et al. (1996), where $\Gamma = h/d$. The resulting equation for the depth-averaged velocity is

$$[19] \qquad u_b = u_* (1.2) (\Gamma/Y)^{3/4} (h_b/h)^{3/4}$$

Depth-averaging the equation of conservation of the fluctuating energy, Ferreira (2005) obtained an algebraic relation for the thickness of the transport layer, graphically expressed in Fig. 10 along with the experimental results of Sumer et al. (1996).

It is apparent that h_b/d is not a direct function of the parameters that characterize the transported, namely, the restitution coefficient and the internal friction angle at the bed as the lines corresponding to different sediment are essentially superimposed in Fig. 10. The influence of the density and the diameter is felt only through Shields parameter. The thickness of the transport layer can be approximated by

$$[20] \qquad \frac{h_b}{d} = 1.7 + 5.5Y$$

3.2.2. Equilibrium concentrations and vertical fluxes

The existence of a frictional layer, across which the shear stress may vary, allowed Ferreira (2005), to determine the mass flux between the bed and the transport layer and the depth-averaged sediment concentration in the latter. The integration of the equation of conservation of momentum in the vertical direction over the frictional layer renders

$$[21] \qquad \partial_t (Z_b) = \phi^{\text{net}}_{3,2} = \frac{g \rho^{(w)} (s-1) \tan(\varphi_b)}{u_b (\rho_b u_x)|_{z=Z_f}} (q_{sb} - q^*_{sb})$$

where Z_f is the elevation of boundary between the frictional and collisional layers (layers **A** and **B** in Fig. 3), $q_{sb} = C_b u_b h_b$ is the volumetric bedload discharge and $q^*_{sb} = C^*_b u_b h_b$ is the equilibrium volumetric bedload discharge. The equilibrium concentration is derived from the following considerations: (i) by definition, one has $T(z = Z_b) = \tau_b \equiv \rho^{(w)} C_f u^2$, where $C_f = (u^*/u)^2$ is the friction factor of the overall flow; (ii) in a steady, equilibrium flow one has $T(z = Z_b) = g \rho^{(w)} (s-1) C^*_b h_b \tan(\varphi_b)$, where C^*_b is the equilibrium concentration; hence, the equilibrium concentration is

$$[22] \qquad C^*_b = \frac{C_f u^2}{g(s-1)\tan(\varphi_b) h_b}$$

3.2.3. Flow resistance

The results of Sumer et al. (1996) allows one for the computation of the friction factor. It is apparent in Fig. 11 that the bed shear stress can be adequately described by $\tau_b \equiv \rho^{(w)} C_f u^2$ provided that the friction coefficient is

$$[23] \qquad C_f = 0.02 \left(\frac{h}{d}\right)^{-1/2} \left(\frac{w_s}{u_*}\right)^{-1/2}$$

for low values of $u_{*/ws}$, where w_s is the fall velocity. Equation [23] is plotted against the data of Sumer et al. (1996) in Fig. 11 and it is shown to be applicable to the most common flow regime, characterized by moderate to large values of h/d. A second flow regime, for low values of h/d, is detected (dashed lines in Fig. 11) but its characterization is out of the scope of the present work.

4. Solutions

4.1. Morphological and textural evolution of gravel- and sand-bedded streams

The results of the model described in Sections 2.3 and 3.1 were compared with laboratory data from a set of experimental tests of aggradation and degradation, performed at the Laboratory of Fluid Mechanics, University of Aberdeen in a 12 m long, 40 cm wide, glass-walled recirculating tilting flume. Details of facilities, instrumentation and experimental procedures can be found in Ferreira (2005). The mathematical reproduction of two laboratorial tests is shown herein. The most relevant initial and boundary conditions of the tests are shown in Table 1.

Laboratory test D1 had an initial stage of sediment recirculation in equilibrium that lasted approximately 8 h at constant discharge. The slope, the sediment discharge (mass and composition), the composition of the bed surface, and the

water depth measured in the recirculation stage constitute the initial conditions for the mathematical model. Sediment recirculation was then disconnected and the bed evolved into an armoured bed. The results of the model can be seen in Figs. 12*a* — time evolution of bed elevation and water depth, Fig. 13*a* — time evolution of the bedload, and Fig. 14*a* — composition of the final bed surface.

The initial conditions of test DA1 are the final, armoured stage of test D1. The sediment discharge, the water depth and the bed surface composition were variables that changed the most. The bed slope was not affected significantly, which is indicative of the protective role of the coarser sediment in the bed. The boundary conditions for test DA1 consist of strong sediment overfeeding at the upstream end. Overfeeding was imposed by means of a conveyor belt loaded with sediment with the composition of the bed substrate. The results of the numerical simulation can be seen in Figs. 12*b*, 13*b,* and 14*b*.

The solution procedure is based on a finite-difference explicit discretization of eqs. [3]–[7]. The discretization scheme closely follows MacCormack's (MacCormack 1969). Being a second-order scheme, spurious oscillations near discontinuities will occur. To achieve a monotone solution at discontinuities, a TVD version is used in which the TVD step incorporates the minmod flux limiter (see Ferreira 2005). Jameson's artificial viscosity is used in the equations of conservation of sediment mass (for a discussion of the scheme see Hirsch 1990). The mesh size was $\Delta x = 0.05$ m for all tests.

In what concerns test D1, the model slightly overestimated the bed degradation while reproducing the water depth correctly (Fig. 12*a*). The predicted bed composition was only slightly coarser that the measured one (Fig. 14*a*). It is concluded that the flow resistance is well modelled but that the phenomenon of hiding is not properly addressed in the formulation of Y_{ck} in eq. [14]. The total bedload discharge is well captured by the model. The evolution of the bedload is essentially correct, but the composition is not well predicted (Fig. 13*a*). This points to the necessity on further experimental work in the formulations for W_k and Y_{ck} in eq. [14].

Since the imposed discharge is of the order of magnitude of the transport capacity, the aggradation process in test DA1 is not in the form of a sharp-edged wave (Fig. 12*b*), a feature well captured by the numerical model. The simulated total bedload discharge does not reflect the measured high variability (Fig. 13*b*). At high times, the bedload discharge appears overestimated as well as the bed elevation at $x = 9.0$. This might indicate that the characteristic scale of bedload propagation, greatly dependant on the formulations for u_b, h_b and, especially, $\phi_{3,2}^{net}$, may be overestimated in the model. The final computed bed composition, with $\beta_I = 0.3$, is finer than the registered one, that is, the initial prearmoured bed is attained faster than what was observed (Fig. 14*b*). This corroborates the hypothesis that the morphological characteristic velocities are overestimated in the model. A sensitivity analysis to the values of β_I may help in understanding if the root of the problem lies on the mixing layer idealization or on the specific parameters employed to characterize it.

4.2. Morphological evolution of geomorphic flows featuring immature debris flow

Modelling geomorphic flows requires the application of models, developed within the shallow-flow paradigm, for which the closure equations express flow and sediment dynamics and morphology characteristic of immature debris flows (see Sect. 3.2).

To evaluate the capability of the model to deal with flows observed in nature, the case study of the Ha! Ha! River 1996 dam-break was chosen. Severe rainstorms scourged southern Québec, Canada, between the 18th and the 21st of July 1996. Because of the overtopping and sequent failure of an earthfill dyke, Ha! Ha! River experienced a significant increase in the peak flood discharge. The dam-break wave, superimposed the hydrologic flood, provoked massive geomorphic impacts in the downstream valley (Lapointe et al. 1998; Capart et al. 2007).

It should be highlighted that the simulation of this extreme flood event represents a highly demanding computational test. Firstly, because the morphologic impacts were unusually pronounced (erosion depths of 20 m and deposition layers of 10 m were registered), which constitutes a challenging test for the underlying conceptual model. For the numerical solution procedure, difficulties arise because of the complex channel geometry, featuring constrictions and enlargements, chutes, and low-slope reaches. As a result, subcritical and supercritical flow regimes may co-exist in the computational domain at a given time. Moreover, flow singularities such as hydraulic jumps or critical flow points can be created and destroyed during the simulation.

The conservation equations included in the model are a generalization of system eqs. [3]–[7] for nonprismatic channels (Ferreira et al. 2005). It is also considered that sediment transport is near capacity (Leal et al. 2006; Fraccarollo and Capart 2002). The solution procedure is based on MacCormack's (1969) scheme. The TVD algorithm revealed inadequate to tackle oscillations born from strong momentum sources such as abrupt slope variations (details in Ferreira 2005). Von Neumann's numerical viscosity was used in its place.

The pre- and post-flood measured bed profiles of the Ha! Ha! River can be seen in Fig. 15, in the reaches where the most important morphologic changes have occurred: downstream of the failed dyke and at a chute known as Chute à Perron. The computed bed profiles, corresponding to the rising limb of the discharge hydrograph, can be seen in the same figure.

It was observed that the dyke was eroded completely and so were the sediment deposits below it down to a depth of about 14 m below the initial bed elevation (Fig. 15, left). Massive incision was registered in all convex profiles. In Chute à Perron, the flood excavated a new channel around the rock outcrop (Lapointe et al. 1998) and severe upstream-progressing erosion took place (Fig. 15, right). The new bed is 20 m below the old river bed in some places.

The model can deal with different flow regimes within the computational domain. In Fig. 16, Froude number profiles, up to 11 shocks (hydraulic jumps) and 10 sonic points (or critical flow points) are observed at the end of the computational procedure employed to attain an initial solution

Table 1. Initial and boundary conditions of gravel-sand bedded tests.

Test	Q (m^3s^{-1})	h_0 (m)	i_0 (–)	Q^*_{b0} (10^{-3} kgs^{-1})	Q_{b1} (10^{-3} kgs^{-1})
D1	0.0135	0.069	0.0025	1.698	0.0
DA1	0.0135	0.072	0.0024	—	5.21

Note: Q, water discharge; h_0, initial water depth; i_0, initial slope; Q^*_{b0}, equilibrium mass sediment discharge; Q_{b1}, sediment discharge imposed at the upstream reach.

Fig. 12. Time evolution of bed elevation (full symbols) and water depth (open symbols). (*a*) Test D1; (*b*) test DA1. Measurements were taken at 3.0 m (■ and □), 6.5 m (◇ and ◆) and at 9.5 m (● and ○) from the inlet.

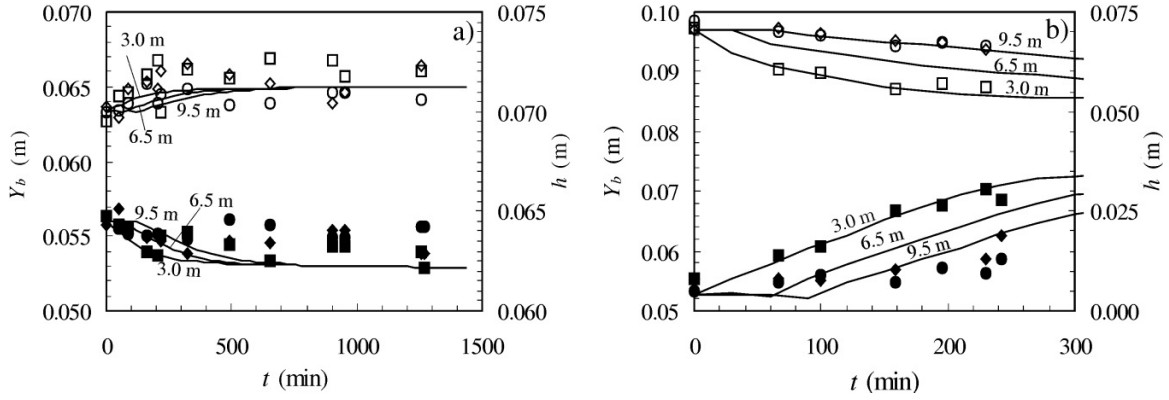

Fig. 13. Time evolution of the bedload discharge Q_b: (*a*) Test D1; (*b*) test DA1. Measurements were taken at 9.0 m from the inlet.

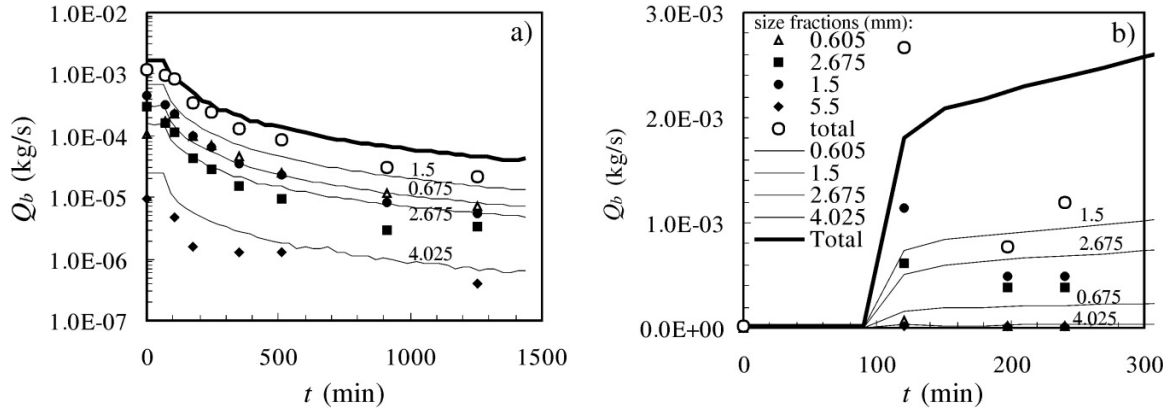

for flow variables, i.e., at t = 0 h (details in Ferreira 2005, 2008, or Ferreira et al. 2005).

Most of the hydraulic jumps and sonic points disappear during the rising limb of the hydrograph. In the same period, one new sonic point and one new hydraulic jump were created at the transition between fixed and mobile bed reaches (kilometre 15). It is noted that the upstream migration of the sonic points is due, as in the case of the knickpoint migration, to the upstream erosion of the point of minimum curvature radius.

The hydraulic jumps identified in Fig. 16, progress in the downstream direction (Leal et al. 2002). This is a consequence of the wave structure of system eqs. [3]–[7]: in mobile bed flows, discontinuities cannot be purely hydrodynamic because the bed elevation or the sediment concentration are dependent variables of the system of conservation laws (further discussion in Ferreira et al. 2006*b*). These hydraulic jumps are associated to a discontinuity in the bed elevation that moves necessarily downstream at a slow velocity until eventually disappearing.

5. Conclusions

Fluvial engineering practice benefits from computational tools for which the phenomenological core are conservation and closure equations, i.e., the conceptual model. The later is drawn from the empirical base of the successful research programs in fluvial processes. Proposals for the conceptual models of two fluvial flow typologies are, in this text, presented. These proposals are based on existent empirical knowledge and on research efforts undertaken by the authors in the past ten years. One of the flow types addressed is that of flat coarse-bed rivers. The other corresponds to geomorphic flows, for which sediment transport is intense, in the form of immature debris flow.

It is argued that both these flows can be idealized as multiple-layered. The conservation equations of both flows can be derived within the continuum shallow-flow paradigm. Furthermore, it is sustained that, in both flow types, sediment transport and flow resistance depend, essentially, on

Fig. 14. Characteristic diameters of the bed surface composition at 6.0 m from the inlet. Simulation results superimposed to initial (- - ○ - -) and final (- -◆- -) bed data in (*a*) test D and (*b*) test DA1. The coordinates are relative to the initial bed for the laboratorial data and for the final bed for the numerical data. From top to bottom characteristic diameters are d_{90}, d_{80}, d_{70}, d_{50}, d_{30}, d_{20}, and d_{10}.

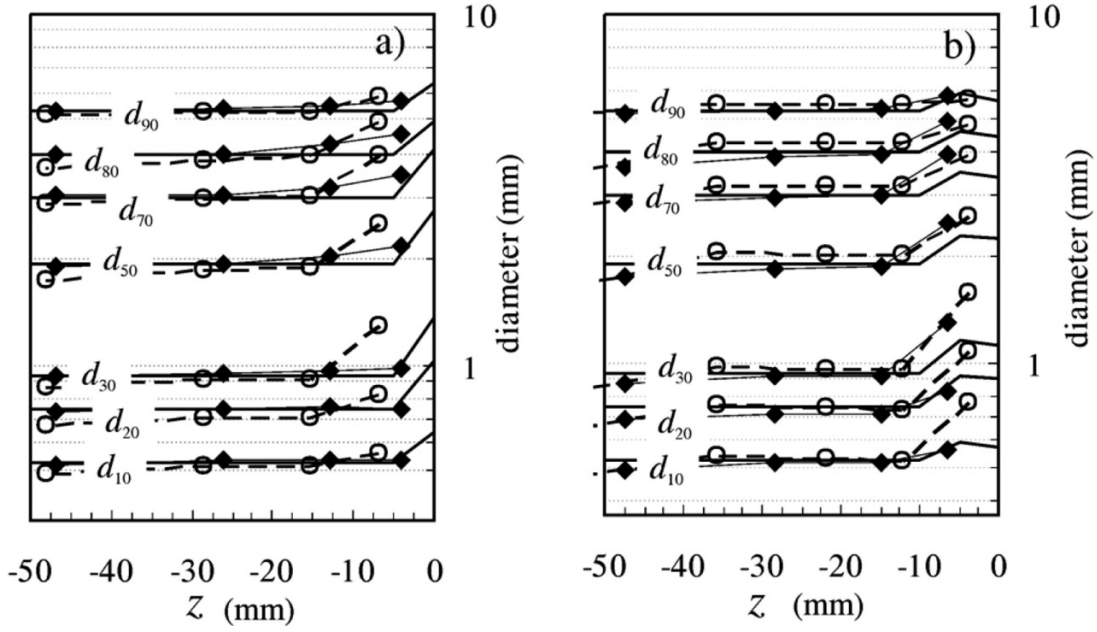

Fig. 15. Morphologic evolution of the Ha! Ha! River between t = 26 and 68 h at two reaches: downstream of the failed dyke (left) and at Chute à Perron (right).

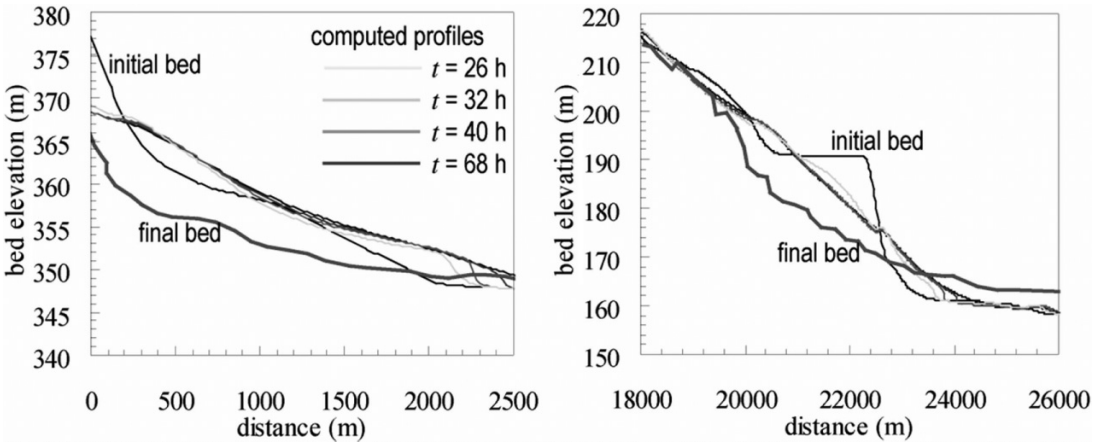

grain-scale phenomena. Bed forms that scale with the flow depth are absent in the flow description. Indeed, bedload transport rates depend on momentum transfer between fluid and individual grains on the bed, in the case of coarse bedded streams (Section 3.1.3), and on the stability of the frictional sublayer, in the case of debris flows (Section 3.2.2). As for flow resistance, it is seen in Section 3.1.1 and 3.1.4 that u_* is much depending on bed texture in coarse bedded streams. In debris flows, flow resistance depends, on collisional and frictional interactions between grains (Sections 3.2 and 3.2.3).

The research efforts presented in Sections 2. and 3. of this text possess strong experimental and theoretical components. Possessing intrinsic empirical value, the results of such research are neverthless mainly employed to build coherent conceptual models in this paper, in which both conservation and closure equations stem from the same theoretical framework.

To illustrate the descriptive potential of the proposed conceptual models, numerical solutions were presented and discussed. One of the simulations concerned the morphological and textural evolution of a sand–gravel channel bed, generated in laboratory. Since the closure equations were derived essentially from laboratorial data obtained in the same channel with the same sediment sizes, the simulation served the purpose of assessing the internal consistency of the model more than proving its predicting abilities. A second numerical simulation was designed to test the predictive capabilities of the conceptual model for geomorphic flows featuring immature debris flow. The results showed that the model can be used in river engineering contexts, mostly because it requires a little amount of field data.

Fig. 16. Profiles of the Froude number. Rrising limb of the discharge hydrograph is shown by top figure. Receding limb is shown by bottom figure. Sonic points signalled by (t = 0 and t = 68 h) or ↓ (t = 26 h); hydraulic jumps signalled by ↓ (t = 0 and t = 68 h) or ↓ (t = 26 h). Thin gray line stands for the initial bed.

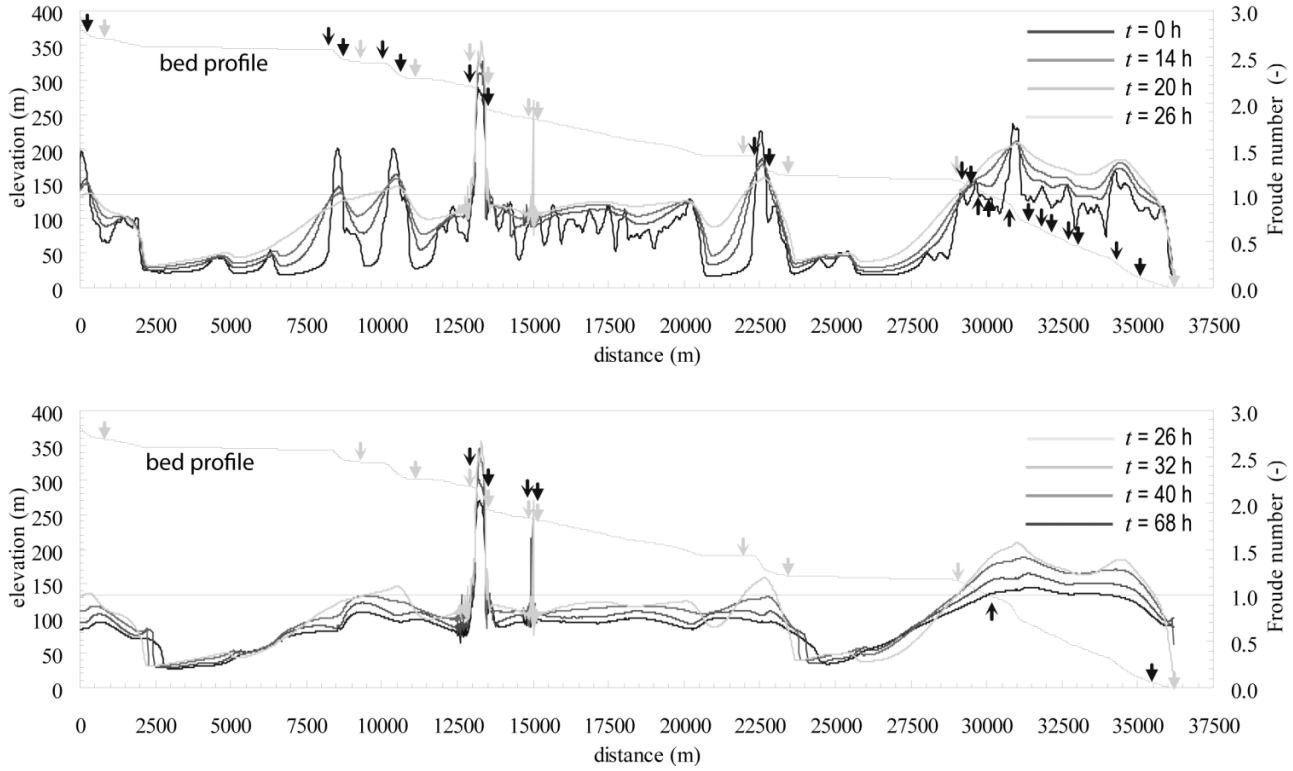

Acknowledgements

The Portuguese Foundation for Science and Technology is acknowledged for the financial support provided through the project PTDC/ECM/65442/2006. The authors thank the two anonymous reviewers whose comments, corrections and suggestions helped clarifying many issues in this paper.

References

Aberle, J. 2006. Spatially averaged near-bed flow field over rough armor layers. *In* River Flow 2006, Lisbon. Taylor and Francis Group, London. Vol. 1, pp. 153–162.

Aberle, J., Koll, K., and Dittrich, A. 2008. Form induced stresses over rough gravel beds. Acta Geophysica, **56**(3): 584–600. doi:10.2478/s11600-008-0018-x.

Armanini, A., Capart, H., Fraccarollo, L., and Larcher, M. 2005. Rheological stratification in experimental free-surface flows of granular–liquid mixtures. Journal of Fluid Mechanics, **532**: 269–319. doi:10.1017/S0022112005004283.

Ascher, U., Mattheij, R., and Russel, R. 1995. Numerical solution of boundary value problems for ordinary differential equations. SIAM, Philadelphia, Pa.

Bagnold, R.A. 1966. An approach to the sediment transport problem for general physics. Professional Paper 422-I. U.S. Geological Survey, Washington, D.C.

Barenblatt, G.I. 1996. Scaling, self-similarity and intermediate asymptotics. Cambridge University Press, Cambridge, UK.

Campbell, C.S. 1989. The stress tensor for simple shear flows of a granular material. Journal of Fluid Mechanics, **203**: 449–473. doi:10.1017/S0022112089001540.

Capart, H., Spinewine, B., Young, D.L., Zech, Y., Brooks, G.R., Leclerc, M., and Secretan, Y. 2007. The 1996 Lake Ha! Ha! breakout flood, Québec: Test data for geomorphic flood routing methods. Journal of Hydraulic Research, **45**: 97–109.

Chapman, S., and Cowling, T.G. 1970. The mathematical theory of non-uniform gases. 3rd ed. Cambridge University Press.

Chiew, Y.-M., and Parker, G. 1994. Incipient sediment motion on non-horizontal slopes. Journal of Hydraulic Research, **32**(5): 649–660.

Cui, Y., Parker, G., and Paola, C. 1996. Numerical simulation of aggradation and downstream fining. Journal of Hydraulic Research, **34**(2): 185–204.

Dittrich, A., and Koll, K. 1997. Velocity field and resistance of flow over rough surface with large and small relative submergence. International Journal of Sediment Research, **12**(3): 21–33.

Einstein, H.A. 1950. The bed load function for sediment transportation in open-channel flows. Bulletin 1026. U.S. Deptartment of Agriculture, Soil Conservation Service.

Ettema, R., and Mutel, C.F. 2004. Hans Albert Einstein: innovation and compromise in formulating sediment transport by rivers. Journal of Hydraulic Engineering, **130**(6): 477–487. doi:10.1061/(ASCE)0733-9429(2004)130:6(477).

Ferreira, R.M.L. 2005. River Morphodynamics and sediment transport: Conceptual model and solutions. Ph.D. thesis, Instituto Superior Técnico, T.U., Lisbon. pp. 23–41, 57–73, 67–73, 86–106, 119, 139–141, 148–149, 211–217, 247, 248–249, 254–255, 250–263, 256, 263–278, 279–280, 281, 480–484, 509–510, 510–523. Available from http://www.civil.ist.utl.pt/~ruif/phdthesis.

Ferreira, R.M.L. 2008. Fundamentals of mathematical modelling of morphodynamic processes: Applicationto geomorphic flows. *In* Numerical Modelling of Hydrodynamics for Water Resources. *Edited by* P. García Navarro and E. Playán. Taylor & Francis. pp. 189–209.

Ferreira, L.S.M. 2008. Impact of sediment overfeeding in gravel-

bedded river's salmonid Habitats. M.Sc. thesis, Instituto Superior Técnico, TU, Lisbon.

Ferreira, R.M.L., Leal, J.G.A.B., and Cardoso, A.H. 2002. Turbulent structures and near-bed sediment transport in open-channel flows. *In* River Flow 2002, Louvain-la-Neuve. A.A. Balkema. Vol. 1, pp. 553–563.

Ferreira, R.M.L., Leal, J.G.A.B., and Cardoso, A.H. 2005. Mathematical modelling of the morphodynamic aspects of the 1996 flood in the Ha! Ha! river. *In* Proceedings of the XXXI IAHR Congress, Seoul, Theme D. pp. 3434–3445 (CD-ROM).

Ferreira, R.M.L., Leal, J.G.A.B., and Cardoso, A.H. 2006*a*. Conceptual model for the bedload layer of gravel bed streams based on laboratory observations. *In* River Flow 2006, Lisbon. Taylor and Francis Group, London. Vol. 1, pp. 947–956.

Ferreira, R.M.L., Leal, J.G.A.B., and Cardoso, A.H. 2006*b*. Conceptual model for the bedload layer of gravel bed streams based on laboratory observations. *In* River Flow 2006, Lisbon. Taylor and Francis Group, London. Vol. 1, pp. 947–956.

Ferreira, R.M.L., Franca, M.J., and Leal, J.G.A.B. 2007. Laboratorial and theoretical study of the mobility of gravel and sand mixtures. *In* Proceedings of the 5th River, Coastal and Estuarine Morphodynamics, RCEM 2007. *Edited by* C.M. Dohmen-Janssen and S.J.M.H. Hulscher. pp. 531–539.

Ferreira, R.M.L., Franca, M.J., and Leal, J.G.A.B. 2008. Flow resistance in open channel flows with mobile hydraulically rough beds. *In* River Flow 2008. Vol. 1. *Edited by* Altinakar et al. pp. 385–394.

Ferreira, R.M.L., Ferreira, L.S.M., Ricardo, A.M., and Franca, M.J. 2009. Imposed sand transport on gravel-bedded streams: Impacts on flow variables and consequences for salmonid spawning sites. River Research and Applications, In press. doi:10.1002/rra.1307.

Finnigan, J.J. 2000. Turbulence in plant canopies. Annual Review of Fluid Mechanics, **32**: 519–571. doi:10.1146/annurev.fluid.32.1.519.

Foufoula-Georgiou, E., and Kumar, P. 1994. Wavelets in geophysics. Academic Press, San Diego, Calif.

Fraccarollo, L., and Capart, H. 2002. Riemann wave description of erosional dam-break flows. Journal of Fluid Mechanics, **461**: 183–228. doi:10.1017/S0022112002008455.

Franca, M.J., and Lemmin, U. 2004. A field study of extremely rough, three-dimensional river flow. *In* Proceedings of the 4th IAHR International Symposium on Environmental Hydraulics. Taylor and Francis Group, London.

Franca, M.J. 2005. A field study of turbulent flows in shallow gravel-bed rivers. Ph.D. thesis, No. 3393, École Polytechnique Fédérale de Lausanne. Available from http://library.epfl.ch/theses/?nr=3393.

Franca, M.J., and Lemmin, U. 2006. Detection and reconstruction of coherent structures based on wavelet multiresolution analysis. *In* River Flow 2006, Lisbon. Taylor and Francis Group, London. Vol. 1, pp. 153–162.

Franca, M.J., Ferreira, R.M.L., and Lemmin, U. 2008. Parameterization of the logarithmic layer of double-averaged streamwise velocity profiles in gravel-bed river flows. Advances in Water Resources, **31**(6): 915–925. doi:10.1016/j.advwatres.2008.03.001.

Giménez-Curto, L., and Corniero Lera, M. 1996. Oscillating turbulent flow over very rough surfaces. Journal of Geophysical Research, **101**: 20745–20758. doi:10.1029/96JC01824.

Grass, A.J. 1971. Structural features of turbulent flow over smooth and rough boundaries. Journal of Fluid Mechanics, **50**(2): 233–255. doi:10.1017/S0022112071002556.

Hirano, M. 1971. River bed degradation with armouring. Transactions of the Japan Society of Civil Engineers, **3**(2): 194–195.

Hirsch, C. 1990. Numerical computation of internal and external flows: Computational methods for inviscid and viscous flows. Vol. 2, 1994 Reprint. Willey-Interscience Publication. pp. 279–281.

Hogg, A.J., Dade, W.B., Huppert, H.E., and Soulsby, R.L. 1996. A model of an impinging jet on a granular bed, with application to turbulent, event-driven bedload transport. *In* Coherent Flow Structures in Open Channels. John Wiley and Sons Ltd. pp. 101–124.

Iverson, R. 1997. The physics of debris flows. Reviews of Geophysics, **35**(3): 245–296. doi:10.1029/97RG00426.

Jenkins, J.T., and Askari, E. 1991. Boundary conditions for rapid flows: Phase interfaces. Journal of Fluid Mechanics, **223**: 497–508. doi:10.1017/S0022112091001519.

Jenkins, J.T., and Hanes, D.M. 1998. Collisional sheet flows of sediment driven by a turbulent fluid. Journal of Fluid Mechanics, **370**: 29–52. doi:10.1017/S0022112098001840.

Jenkins, J.T., and Richman, M.W. 1985. Kinetic theory for plane flows of a dense gas of identical, rough, inelastic circular disks. Physics of Fluids, **28**(12): 3485–3494. doi:10.1063/1.865302.

Jenkins, J.T., and Richman, M.W. 1988. Plane simple shear of smooth inelastic circular disks: the anisotropy of the second moment in the dilute and dense limits. Journal of Fluid Mechanics, **192**: 313–328. doi:10.1017/S0022112088001879.

Jenkins, J.T., and Savage, S.B. 1983. A theory for the rapid flow of identical smooth, nearly elastic, spherical particles. Journal of Fluid Mechanics, **130**: 187–202. doi:10.1017/S0022112083001044.

Koll, K. 2006. Parameterization of the vertical profile in the wall region over rough surfaces. *In* River Flow 2006, Lisbon. Taylor and Francis Group, London. Vol. 1, pp. 153–162.

Lapointe, M.F., Secretan, Y., Driscoll, S.N., Bergeron, N., and Leclerc, M. 1998. Response of the Ha! Ha! River to the flood of July 1996 in the Saguenay region of Quebec: Large-scale avulsion in a glaciated valley. Water Resources Research, **34**: 2383–2392. doi:10.1029/98WR01550.

Leal, J.G.A.B., Ferreira, R.M.L., and Cardoso, A.H. 2002. Dam-break waves on movable bed. *In* River Flow 2002, Louvain-la-Neuve. A.A. Balkema. Vol. 2, pp. 981–990.

Leal, J.G.A.B., Ferreira, R.M.L., and Cardoso, A.H. 2006. Dam-break wave front celerity. Journal of Hydraulics Engineering, ASCE, **132**(1): 69–76. doi:10.1061/(ASCE)0733-9429(2006)132:1(69).

Lun, K.K., Savage, S.B., Jeffrey, D.J., and Chepurny, N. 1984. Kinetic theories for granular flows: Inelastic particles in Couoette flow and slightly inelastic particles in a general flow field. Journal of Fluid Mechanics, **140**: 223–256. doi:10.1017/S0022112084000586.

MacCormack, R.W. 1969. The effect of viscosity in hypervelocity impact cratering. Paper 69-354. American Institute of Aeronautics and Astronautics.

Meyer-Peter, E., and Müller, R. 1948. Formulas for bed-load transport. *In* Report on Second Meeting of International Association for Hydraulic Research, Stockholm, Sweden. pp. 39–64.

Nakagawa, H., and Nezu, I. 1977. Prediction of the contribution to the Reynolds stress from bursting events in open-channel-flows. Journal of Fluid Mechanics, **80**(1): 99–128. doi:10.1017/S0022112077001554.

Neill, C.R., and Yalin, M.S. 1969. Qualitative definition of beginning of bed movement. Journal of the Hydraulics Division, **95**(1): 585–587.

Nelson, J.M., McLean, S.R., and Wolfe, S.R. 1993. Mean flow and turbulence over two-dimensional bed forms. Water Resources Research, **29**: 3935–3953. doi:10.1029/93WR01932.

Nikora, V. 2008. Hydrodynamics of rough-bed turbulent flows: spatial averaging perspective. In *River Flow 2008.* Vol. 1. *Edited by* Altinakar et al. pp. 11–19.

Nikora, V., Goring, D., McEwan, I., and Griffiths, G. 2001. Spatially averaged open-channel flow over rough bed. Journal of Hydraulics Engineering, ASCE, **127**(2): 123–133. doi:10.1061/(ASCE)0733-9429(2001)127:2(123).

Niño, Y., Garcia, M., and Ayala, L. 1994. Gravel saltation, 1: Experiments. Water Resources Research, **30**(6): 1907–1914. doi:10.1029/94WR00533.

Ogawa, S. 1978. Multitemperature theory of granular materials. *In* Proceedings of the US–Japan Symposium on Continuum Mechanics and Statistical Approaches to the Mechanics of Granular Media. *Edited by* S. Cowin and M. Satake, Gakujutsu Bunken Fukyu-kai, Tokyo, pp. 208–217.

Owen, P.R. 1964. Saltation of uniform grains in air. Journal of Fluid Mechanics, **20**(2): 225–242. doi:10.1017/S0022112064001173.

Parker, G. 1991. Selective sorting and abrasion of river gravel, I: Theory. Journal of Hydraulic Engineering, **117**(2): 131–149. doi:10.1061/(ASCE)0733-9429(1991)117:2(131).

Phillips, B., and Sutherland, A. 1989. Spatial lag effects in bed load sediment transport. Journal of Hydraulic Research, **27**(1): 115–133.

Pokrajac, D., McEwan, I., and Nikora, V. 2008. Spatially averaged turbulent stress and its partitioning. Experiments in Fluids, **45**: 73–83. doi:10.1007/s00348-008-0463-y.

Pöschel, T., Brilliantov, N.V., and Schwager, T. 2002. Violation of molecular chaos in dissipative gases. International Journal of Modern Physics C, **13**(9): 1263–1272. doi:10.1142/S012918310200411X.

Savage, S.B. 1979. Gravity flow of cohesionless granular materials in chutes and channels. Journal of Fluid Mechanics, **92**: 53–96. doi:10.1017/S0022112079000525.

Savage, S.B., and Hutter, K. 1989. The motion of a finite mass of granular material down a rough incline. Journal of Fluid Mechanics, **199**: 177–215. doi:10.1017/S0022112089000340.

Savage, S.B., and Jeffrey, D.J. 1981. The stress tensor in a granular flow at high shear-rates. Journal of Fluid Mechanics, **110**: 255–272. doi:10.1017/S0022112081000736.

Sumer, B.M., Kozakiewicz, A., Fredsøe, J., and Deigard, R. 1996. Velocity and concentration profiles in sheet-flow layer of movable bed. Journal of Hydraulic Engineering, **122**: 549–558. doi:10.1061/(ASCE)0733-9429(1996)122:10(549).

Sutherland, A.J. 1967. Proposed mechanism for sediment entrainment by turbulent flows. Journal of Geophysical Research, **72**(24): 6183–6194. doi:10.1029/JZ072i024p06183.

Toro-Escobar, C.M., Parker, G., and Paola, C. 1996. Transfer function for the deposition of poorly sorted gravel in response to streambed aggradation. Journal of Hydraulic Research, **34**(1): 35–53.

Townsend, A.A. 1976. The structure of turbulent shear flows. 2nd ed. Cambridge University Press. Cambridge, UK. pp. 139–150.

Wilcock, P.R., Kenworthy, S., and Crowe, J. 2001. Experimental study of the transport of mixed sand and gravel. Water Resources Research, **37**(12): 3349–3358. doi:10.1029/2001WR000683.

Yalin, M.S. 1963. An expression for bed load transport. Journal of the Hydraulics Division, **89**(3): 221–250.

Yalin, M.S. 1971. Theory of hydraulic models. MacMillan, New York. pp. 145–186.

Yalin, M.S. 1977. Mechanics of sediment transport. 2nd ed. Pergamon Press, UK.pp. 54–73.

Yalin, M.S. 1992. River mechanics. Pergamon Press, UK.